

## Exploring the degradation behavior of MgXAg alloys by in vitro electrochemical methods

Yuqiuhan Zhang, Tycho Zimmermann, Wolf-Dieter Mueller<sup>\*</sup>, Frank Witte, Florian Beuer, Andreas Schwitalla

Charité – Universitätsmedizin Berlin, corporate member of Freie Universität Berlin and Humboldt-Universität zu Berlin, Dental Materials and Biomaterial Research, Department of Prosthodontics, Geriatric Dentistry and Craniomandibular Disorders, Aßmannshäuser Str. 4-6, 14197, Berlin, Germany

### ARTICLE INFO

#### Keywords:

Biodegradable magnesium  
Magnesium silver alloys  
Electrochemistry  
Hydrogen evolution

### ABSTRACT

Magnesium as biodegradable biomaterial could serve as bone augmentation material in implant dentistry. The knowledge about the predictability of the biodegradation process is essential as this process needs to go hand in hand with the formation of new bone to gradually replace the augmentation material. Therefore, this work aimed to assess if the electrochemistry (EC) measurements of the corrosion process correlate with the surface features at various time points during the surface degradation, in order to describe the degradation process of Mg and Mg alloys more reliably, under the assumption that differences in EC behavior can be detected and related to specific patterns on the surface.

In this test setup, a special optical chamber was used for electrochemical measurements on Mg and Mg-alloys (Mg2Ag, Mg4Ag, and Mg6Ag). Specimens were investigated using different circulating cell culture solutions as electrolytes, these were minimum essential medium (MEM), Hank's Balanced Salt Solution (HBSS), and MEM+ (MEM with added sodium hydrogen carbonate) at 37 °C. Open circuit potential measurements (OCP) over 30 min followed by cyclic polarization were performed. The electrochemistry data, including OCP, exchange current density and corrosion potential, were compared with visible changes at the surface during these treatments over time. The results show that the addition of silver (Ag) leads to a “standardization” of the degradation regardless of the selected test medium. It is currently difficult to correlate the visible microscopic changes with the data taken from the measurements. Therefore, further investigations are necessary.

### 1. Introduction

Magnesium used as a base metal for implantable devices has a number of favorable properties such as a low density, the possibility to manufacture tiny structures, easiness of manipulation during surgery, the properties of its degradation products (Mg<sup>2+</sup>ions) to promote the deposition of calcium and phosphorus and the growth of compact bones [1] as well as its complete degradation and absorption, making a second operation unnecessary, e.g. when used as osteosynthesis material [2].

Compared to other biodegradable metals like zinc or iron, magnesium is chemically more reactive. The rapid degradation in a humid physiological environment remains the main obstacle to widespread use, as it leads to rapid loss of mechanical integrity followed by the structural collapse of the magnesium-based implant, possibly even before the bone

has healed to a structurally sound degree [3,4].

Magnesium and Mg-alloys preferentially degrade non-uniformly [5]. This is due to a complex degradation behavior and is based on the galvanic coupling occurring where the anodic and the cathodic partial reaction of the redox-reaction system take place on the same surface area [6]. The consequence thereof is, that over the surface in contact with the electrolyte (the body fluid or simulated body fluid) one part of the surface is oxidized and degraded due to the anodic reaction (1), while the two electrons are transferred to the cathodic partial reaction, where hydrogen evolution (HE) takes place (2). The Hydrogen evolution reaction (HER) is the main cathodic reaction during magnesium corrosion and occurs spontaneously [30–32]. Furthermore, the overall reaction consumes H<sup>+</sup> ions causing a higher concentration of OH<sup>-</sup> ions (3), thus an increased pH in the physiological electrolyte, causing

Peer review under responsibility of KeAi Communications Co., Ltd.

<sup>\*</sup> Corresponding author.

E-mail addresses: [yuqiuhan.zhang@charite.de](mailto:yuqiuhan.zhang@charite.de) (Y. Zhang), [tycho.zimmermann@charite.de](mailto:tycho.zimmermann@charite.de) (T. Zimmermann), [wolf-dieter.mueller@charite.de](mailto:wolf-dieter.mueller@charite.de) (W.-D. Mueller), [frank.witte@charite.de](mailto:frank.witte@charite.de) (F. Witte), [florian.beuer@charite.de](mailto:florian.beuer@charite.de) (F. Beuer), [andreas.schwitalla@charite.de](mailto:andreas.schwitalla@charite.de) (A. Schwitalla).

<https://doi.org/10.1016/j.bioactmat.2021.05.044>

Received 21 November 2020; Received in revised form 3 May 2021; Accepted 26 May 2021

Available online 10 June 2021

2452-199X/© 2021 The Authors. Publishing services by Elsevier B.V. on behalf of KeAi Communications Co. Ltd. This is an open access article under the CC

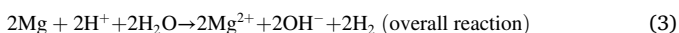
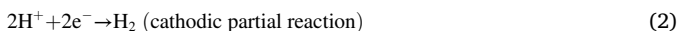
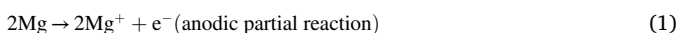
BY-NC-ND license (<http://creativecommons.org/licenses/by-nc-nd/4.0/>).

**Table 1**

The major components of MEM, HBSS and MEM plus (formulations offered by manufacturer).

	MEM (g/L)	HBSS (g/L)	MEM Plus (g/L)
NaCl	6.8	8	6.68
CaCl <sub>2</sub>	0.2	0.14	0.2
KCl	0.4	0.4	0.4
CaCl <sub>2</sub>	0.2	0.14	0.2
MgSO <sub>4</sub>	0.97	0.098	0.2
NaH <sub>2</sub> PO <sub>4</sub>	0.14	0.06	0.14
Special additives	w/o Phenol red Vitamins Amino acids w/ oNaHCO <sub>3</sub>	w/o Phenol red w/o Amino acids NaHCO <sub>3</sub> 0.35 KH <sub>2</sub> PO <sub>4</sub> 0.06 MgCl <sub>2</sub> 1.0	w/o Phenol red Vitamins Amino acids +0.35 g/L NaHCO <sub>3</sub>

precipitation of magnesium phosphate and carbonate [7]. In the next step, the dissolved Mg<sup>+</sup> and the OH<sup>-</sup> ions precipitate as magnesium hydroxide layer on the surface of the Mg or Mg alloys (4) [5,8].



Silver has been used by humans for thousands of years due to its strong antibacterial effects. Already under Alexander the Great’s reign, silver vessels were used to store drinking water and food [9]. The formulation of silver has evolved from bulk silver in vessels and coins to ionic silver supplemented as silver salts (such as AgNO<sub>3</sub>) or adsorbed on carrier materials [10]. Silver exhibits low toxicity in the human body, and minimal risk is expected due to clinical exposure by inhalation, ingestion, dermal application or through the urological or hematogenous route [11]. Innovative binary Mg–Ag alloys were built as bone implant material to add antibacterial properties to biodegradable magnesium. When combined with its propensity to degrade in physiological conditions, the antibacterial property may last for the duration of the implant. Among the criteria for determining biocompatibility and antibacterial reaction [12], the various corrosion rates from α and β phases influence the corrosion mechanism [13]. The corrosion potential of Mg–Ag metal compounds is shifted in an anodic direction by adding silver. Because these complex interactions remain a critical concern, it is important to explore the corrosion behavior of magnesium-silver alloys in detail [14,15].

For in vitro experiments to study the biodegradation of Mg and Mg alloys, various types of simulated body fluids have been used [27,28]. So far, there is no clear consensus on the best type of environment to simulate physiological in vivo conditions [16]. The corrosive environment of Mg in the human body is composed of 0.14 M NaCl solution and a small amount of other inorganic substances (such as Ca<sup>2+</sup>, PO<sub>4</sub><sup>3-</sup> and HCO<sub>3</sub><sup>-</sup>) [17]. The normal pH of blood is 7.4, generally buffered by the CO<sub>2</sub>/HCO<sub>3</sub><sup>-</sup> system [18]. The presence of chloride ions usually leads to accelerated corrosion [19], since the formation of MgCl<sub>2</sub> releases OH<sup>-</sup> ions from the precipitation layer (5), which in turn can react with the

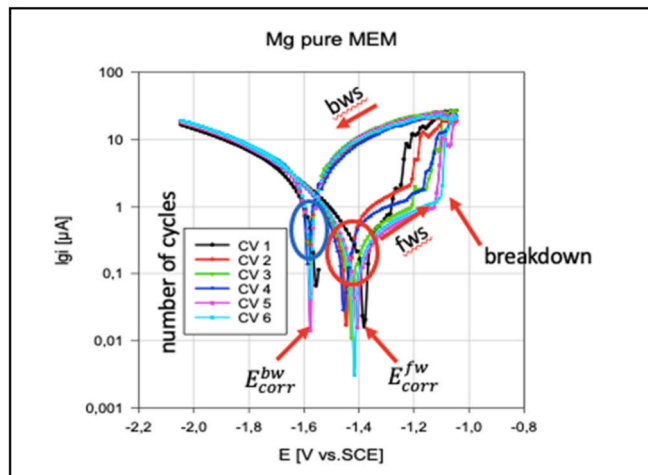
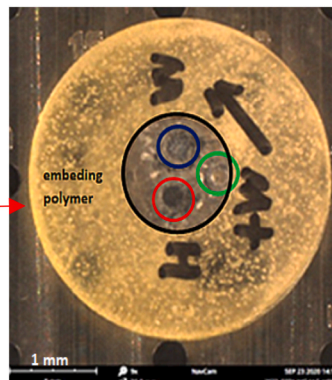
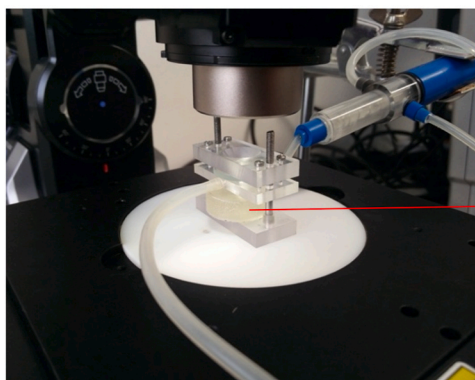


**Fig. 2.** Description of I vs. E curves (The blue circle marks the range of backward scan for assessing I<sub>corr</sub>, the red circle for the forward scan and the red arrows marked the scan direction and points of interest.). (For interpretation of the references to color in this figure legend, the reader is referred to the Web version of this article.)

**Table 2**

Surface roughness of specimens after polishing.

materials	Sa (left)	Sa (right)	Sa (up)	Sa (down)	Sa (middle)	±SD (Sa)
Mg2Ag (μm)	1.426	1.688	1.706	1.523	1.747	0.1371
Mg4Ag (μm)	1.018	1.233	0.963	1.034	1.187	0.1163
Mg6Ag (μm)	1.352	0.932	1.097	0.908	1.138	0.1796
Mg XHP	1.316	1.313	1.337	1.328	1.329	0.0099
Mg Pure	1.341	1.298	1.327	1.305	1.315	0.0172



microscopic view of the position of the measurement areas onto the surface of the specimen

Red – HBSS  
Green – MEM+  
Blue – MEM  
Black – specimen

**Fig. 1.** left: electrochemical flow chamber under the video-microscope (magnification x135) right: the measurement areas on the surface of the specimen for each of the electrolytes.

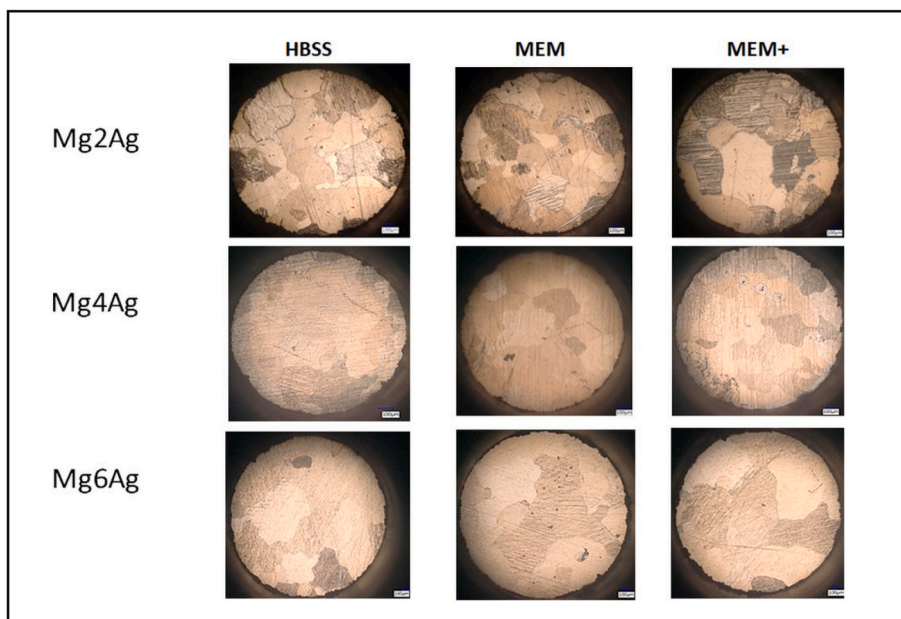


Fig. 3. Initial states of MgXAg alloys before the electrochemical measurements in HBSS – MEM and MEM+.

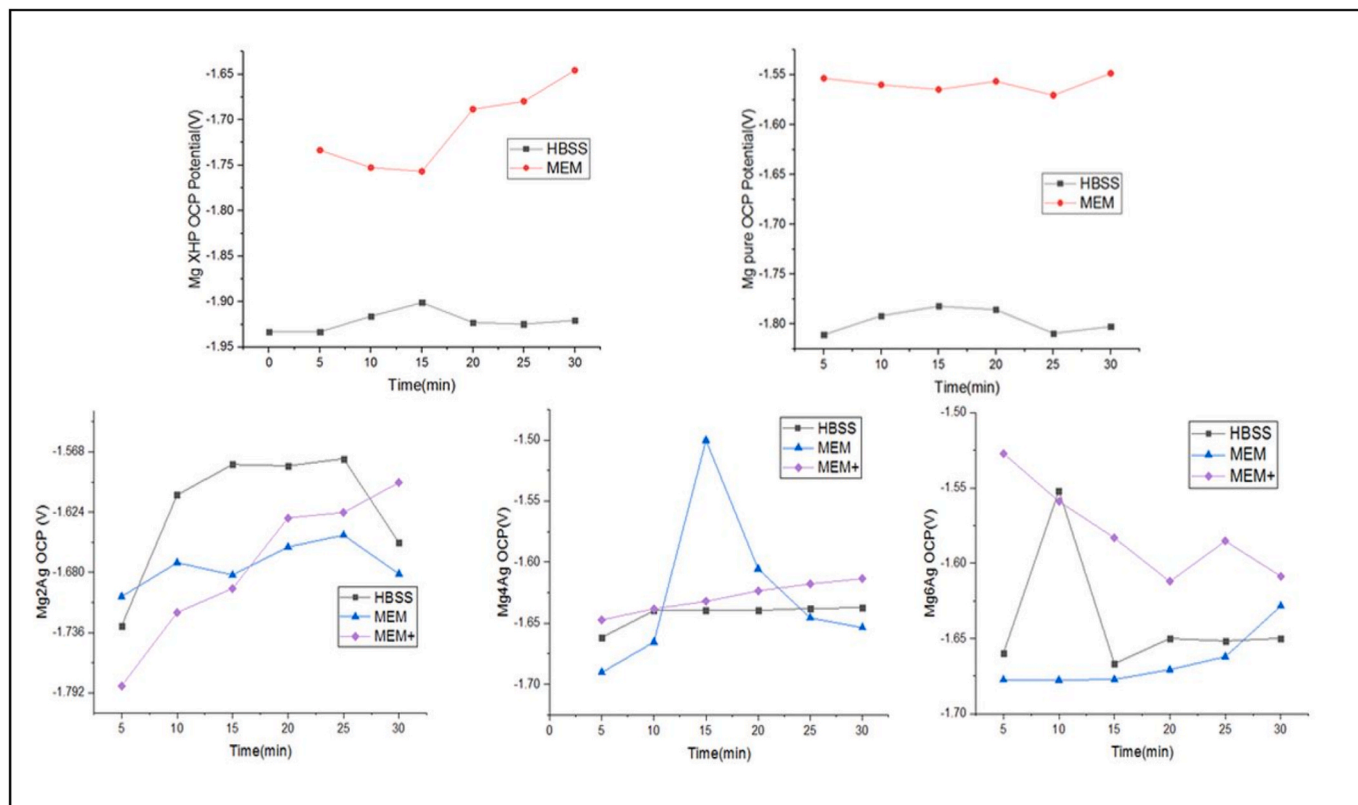


Fig. 4. Comparison of the OCP vs. time curves of Mg XHP and Mg pure on the top and MgXAg (from left to right: 2Ag, 4Ag, 6Ag) in MEM, HBSS and MEM+ at 37 °C in a flow chamber.

**Table 3**  
Final potential(V) after 30 min OCP in 3 different electrolytes.

Mg/Mg alloys	Mg XHP	Mg pure	Mg2Ag	Mg4Ag	Mg6Ag
HBSS	-1.920	-1.802	-1.652	-1.637	-1.649
MEM	-1.645	-1.768	-1.681	-1.653	-1.628
MEM+			-1.596	-1.613	-1.608

dissolved  $Mg^{2+}$  ions, while phosphates and carbonates may promote the formation of protective or partially protective corrosion products [12]. The presence of organic components, such as proteins, cells, or bacteria, can additionally affect the corrosion reaction [20]. Compared to room temperature, the body temperature of 37 °C can accelerate the corrosion reaction on the one hand and modify it to some extent on the other, since the solubility of calcium phosphate is also dependent on the temperature

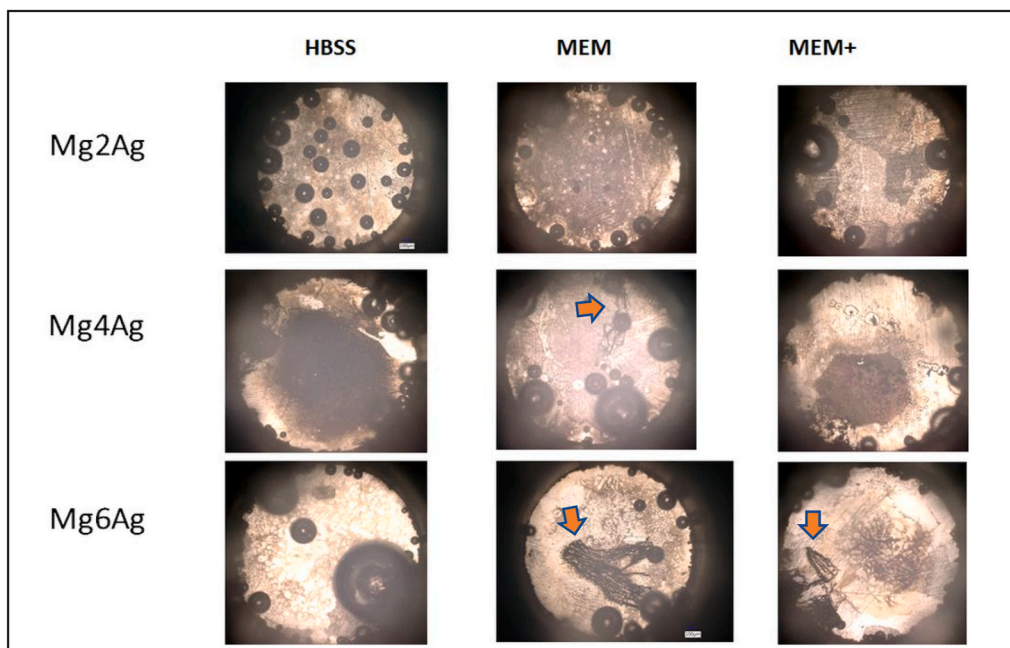


Fig. 5. situation at the surface of MgXAg alloys after OCP measurements over 30 min in HBSS – MEM and MEM+. Initial degradation is marked by red arrows. (For interpretation of the references to color in this figure legend, the reader is referred to the Web version of this article.)

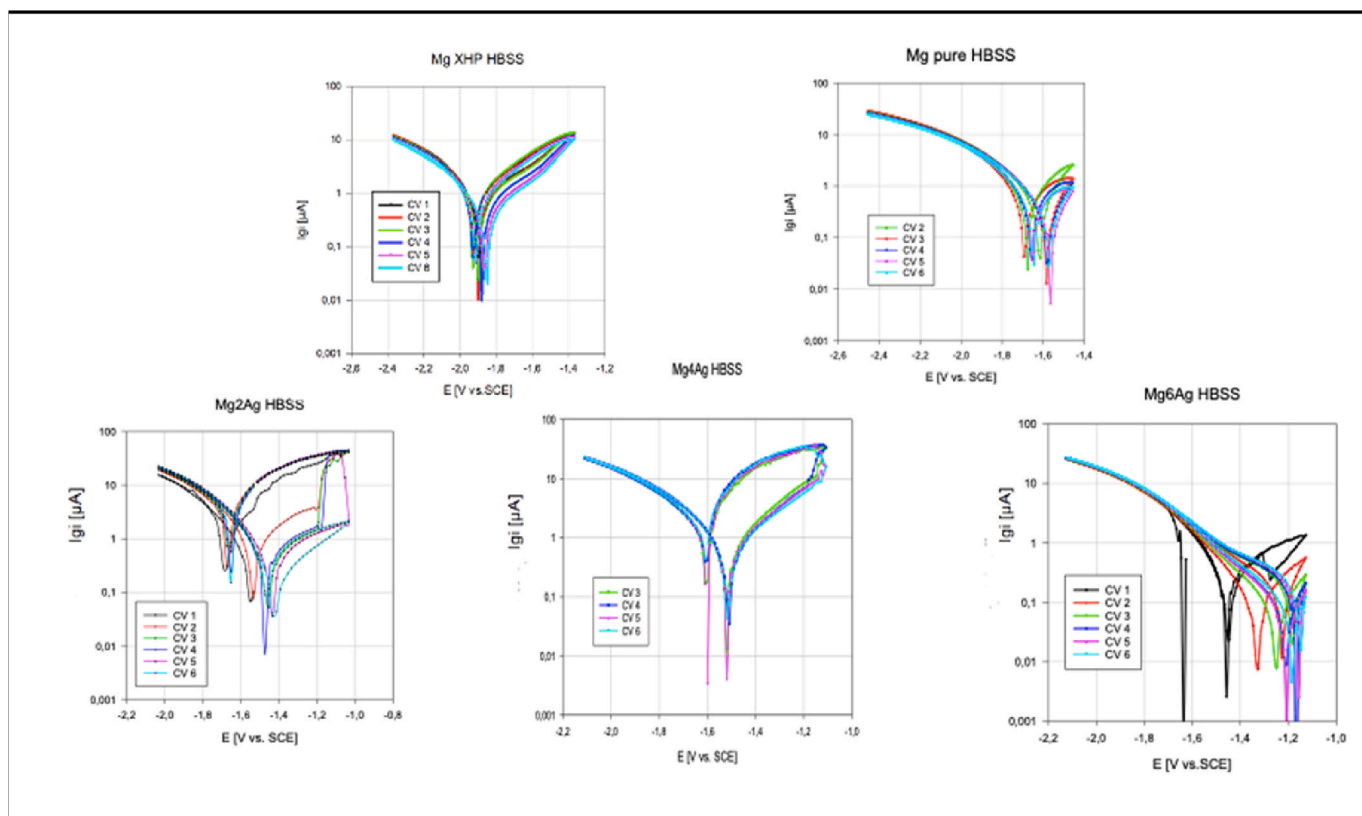


Fig. 6a. Comparison of the electrochemical behavior of Mg XHP and Mg pure in HBSS (top) and MgXAgalloys (bottom) at 37 °C in a flow chamber.

[21]. These different influencing factors deriving from the bodily environment make investigations of the corrosion process very complex and thus challenging.

The results of many literature outcomes have plainly showed that the consumption of Mg is exceptional regarding its electrochemical behavior. In nature, the corrosion of Mg and its alloys is an

electrochemical process, and their corrosion performance or characteristics can be ultimately attributed to their electrochemical behavior. Revealing the electrochemical reactions involved in the corrosion process can provide a theoretical basis for understanding the characteristic corrosion phenomena for Mg and its alloys [22]. Therefore, the study aimed to correlate electrochemical (EC) measurements with surface

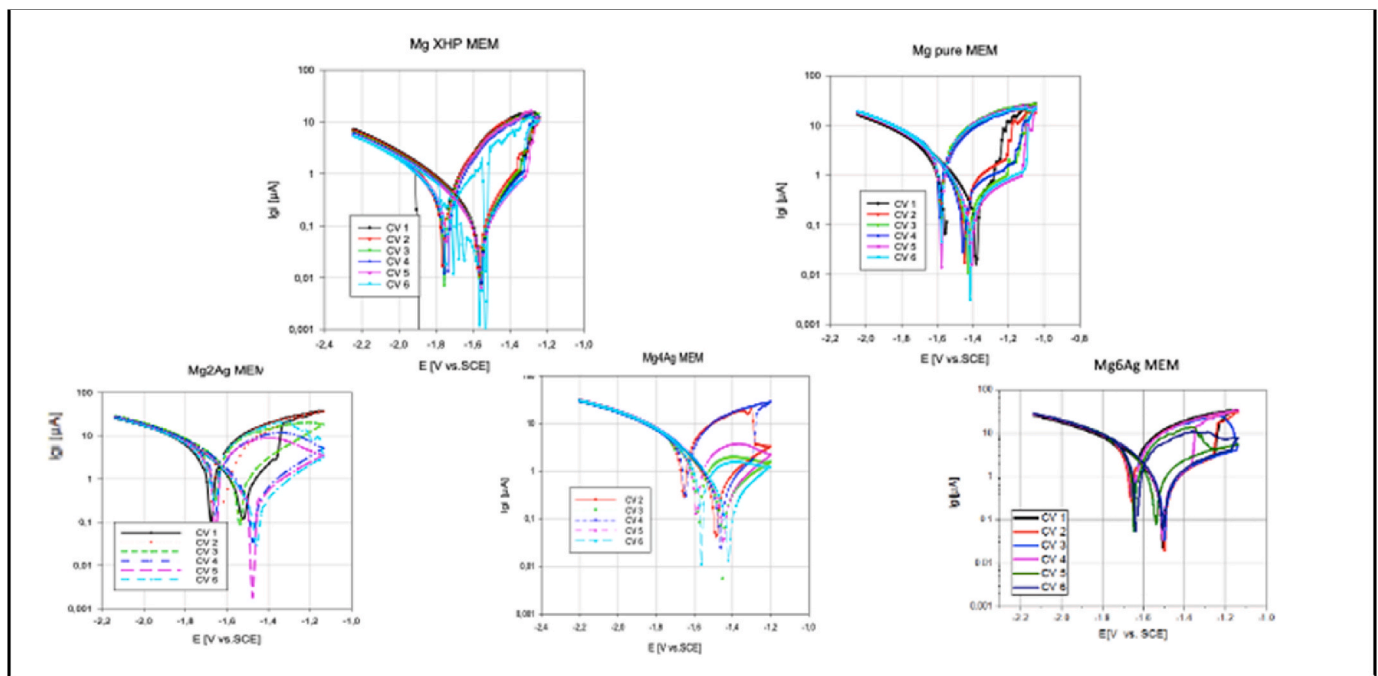


Fig. 6b. Comparison of the I vs. E curves of cyclic polarization of Mg XHP and Mg pure in MEM (top) and MgXAg alloys (bottom) at 37 °C in a flow chamber.

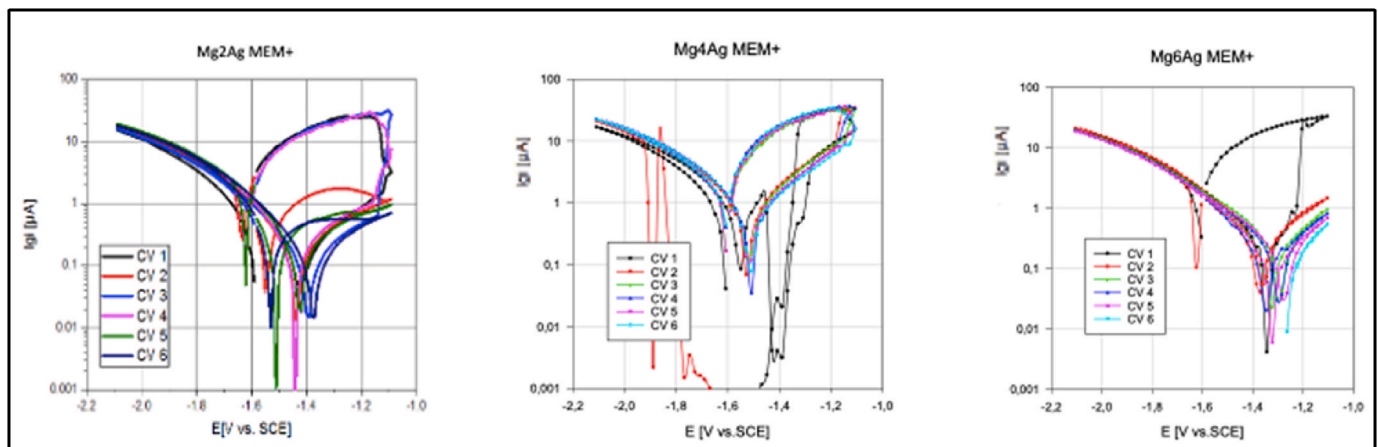


Fig. 6c. Comparison of the I vs. E curves of cyclic polarization of MgXAg in MEM + at 37 °C in a flow chamber (the drop down in the curves in case of Mg4Ag is caused by loss of electrical connection by hydrogen gas bubbles adhering to the surface of the specimen).

changes at different points in time under the influence of three different electrolytes based on the cell culture medias HBSS and MEM to predict the degradation process more reliably.

## 2. Material and method

In these experiments, MEM (Biochrom GmbH, Germany) and HBSS (Life Technologies Limited, UK) buffers, commonly used in the literature, were selected. In contrast to MEM, where amino acids and vitamins are added to the basic ingredients, HBSS contains additional  $\text{NaHCO}_3$  (Sigma-Aldrich Chemie GmbH, Germany), as shown in Table 1. To better compare the corrosion process, in the MEM Plus group 0.35 g/L sodium bicarbonate was added.

Mg XHP (purity: 99.99%) and Mg pure (purity: 99%), as well as three Mg-Ag alloys - Mg2Ag, Mg4Ag and Mg6Ag which contain 1.87%, 3.82% and 6.00% silver and 98%, 96% and 94% magnesium by weight, respectively - were cast and processed with solution T4. All specimens were cylindrical with a diameter of 10 mm and a thickness of 5 mm. In

order to describe the initial degradation process in a time frame of 1 h, an optical coupled electrochemical measurement set up was used [24].

### 2.1. Preparation of magnesium specimens

Mg XHP, Mg pure and MgXAg (X = 2,4,6) samples were prepared by partial encapsulation in an epoxy resin to keep the sample intact during grinding. The surface was ground from 800 till 2500 using silicon carbide sandpaper (150 mm Hermes, Germany) with water, then polished with 1.0  $\mu\text{m}$  silica suspension and etched by a solution, mainly consisting of glacial acetic acid and picric acid, for 10 s for each specimen. Afterwards, the surface of the specimens was washed with ethanol and dried.

### 2.2. Grain size and roughness measurement

For comparison of the surface conditions the specimens were inspected using a video microscope (Keyence VHX-5000, Japan) and the

**Table 4**

The mean values ± SD of  $E_{corr}$  and  $i_{corr}$  data from 5 cycles forward and backward scan of Mg and MgXAg in HBSS, MEM and MEM + at 37 °C under flow conditions.

forward	I [A] HBSS	E [V vs SCE]	I [A] MEM	E [V vs SCE]	I [A] MEM+	E [V vs SCE]
Mg2Ag	$2.2 \times 10^{-5}$ $\pm 1.49 \times 10^{-5}$	-1.508 $\pm 0.092$	$3.73 \times 10^{-5}$ $\pm 4.74 \times 10^{-5}$	-1.513 $\pm 0.052$	$6.15 \times 10^{-6}$ $\pm 1.19 \times 10^{-6}$	-1.414 $\pm 0.028$
Mg4Ag	$5.63 \times 10^{-5}$ $\pm 4.59 \times 10^{-5}$	-1.515 $\pm 0.023$	$1.41 \times 10^{-5}$ $\pm 4.23 \times 10^{-6}$	-1.458 $\pm 0.022$	$2.26 \times 10^{-5}$ $\pm 1.53 \times 10^{-6}$	-1.526 $\pm 0.018$
Mg6Ag	$4.2 \times 10^{-6}$ $\pm 2.37 \times 10^{-6}$	-1.270 $\pm 0.10$	$2.86 \times 10^{-5}$ $\pm 3.67 \times 10^{-6}$	-1.509 $\pm 0.015$	$7.35 \times 10^{-5}$ $\pm 2.13 \times 10^{-6}$	-1.304 $\pm 0.037$
pure	$\pm 4.94 \times 10^{-6}$	-1.597	$\pm 2.65 \times 10^{-5}$	-1.467		
XHP	$\pm 5.48 \times 10^{-6}$	-1.878	$\pm 1.19 \times 10^{-6}$	-1.560		
backward						
Mg2Ag	$8.62 \times 10^{-6}$ $\pm 5.44 \times 10^{-6}$	-1.297 $\pm 0.07$	$1.27 \times 10^{-5}$ $\pm 4.60 \times 10^{-6}$	-1.435 $\pm 0.014$	$5.94 \times 10^{-6}$ $\pm 1.88 \times 10^{-6}$	-1.415 $\pm 0.02$
Mg4Ag	$5.59 \times 10^{-5}$ $\pm 2.90 \times 10^{-5}$	-1.419 $\pm 0.02$	$7.28 \times 10^{-6}$ $\pm 1.93 \times 10^{-6}$	-1.371 $\pm 0.019$	$2.4 \times 10^{-5}$ $\pm 5.57 \times 10^{-6}$	-1.495 $\pm 0.022$
Mg6Ag	$1.1 \times 10^{-5}$ $\pm 6.41 \times 10^{-6}$	-1.378 $\pm 0.04$	$7.4 \times 10^{-5}$ $\pm 1.49 \times 10^{-5}$	-1.493 $\pm 0.034$	$5.26 \times 10^{-6}$ $\pm 1.30 \times 10^{-6}$	-1.279 $\pm 0.042$
pure	$\pm 3.30 \times 10^{-6}$	-1.674	$\pm 2.45 \times 10^{-5}$	-1.575		
XHP	$\pm 3.06 \times 10^{-6}$	-1.924	$\pm 1.00 \times 10^{-6}$	-1.751		

roughness at 5 spots of each specimen was measured using an IF-microscope (Alicona, Austria).

**2.3. Electrochemical measurements**

For electrochemical measurements, the specimens were connected to a copper wire using a silver amalgam. The reactions at the surface of the specimens were observed using a video microscope (Keyence VHX-5000) through a special electrochemical cell [24] (Fig. 1). The electrochemical data were manipulated and accumulated by the software PStrace (PalmSens, Netherlands) connected to a mini-potentiostat (Emstat3+, PalmSens, Netherlands). The solutions were pumped through the system using a lab pump (Watson Marlow 5050Di, United Kingdom). The speed was set as 4.3 ml/min and the temperature was set

to 37 °C (310K). The OCP (open circuit potential) was measured over 30min followed by cyclic polarization over 6 cycles between a potential range of ±500 mV vs. OCP (open circuit potential). The microscopic video observations during the measurements were recorded with OBS Studio (version 26.0.2). Scanning Electron Microscope (SEM) pictures were made by Desktop SEM Phenom XL G2 (Thermo Fisher Scientific, America). The specimens were washed in pure alcohol and blow dried before SEM.

**2.4. Data collection and analysis**

From each of the cyclic I-E curve the exchange current density  $i_{corr}$  was determined at  $E_{corr}$ . The body temperature of 310K, the number of the transferred electrons per reaction ( $n = 2$ ), the Faraday’s constant  $F$  with  $.96485 \text{ As}\cdot\text{mol}^{-1}$  as well as the Stern-Geary-Coefficient with 0.01335 were used in equation (6), the linearized Butler-Volmer equation.

$$I_0 = \frac{RT}{nFR_p} = \frac{\text{Stern - Geary - Coefficient}}{R_p} (\text{A}/\text{cm}^2) \tag{6}$$

One example of a specific I vs E cyclic curve with the marked data points is shown in Fig. 2.

**3. Results**

**3.1. Roughness measurements**

The roughness values of the investigated specimens are comparable, as the data show in Table 2. Mg2Ag shows the highest roughness followed by both pure Mg specimens and then Mg4Ag and Mg6Ag.

The pictures in Fig. 3 show the initial states of the surface of the MgXAg alloys prepared for the electrochemical measurements in HBSS, MEM and MEM+.

**3.2. Electrochemical measurements**

In all cases the OCP values starts from a very cathodic point and after the first 5 min reach a value which was more or less constant over the rest of the measurement time up to 30 min as shown for the different investigated alloys in Fig. 4.

Contrary to expectations, no major differences were found for the OCP for the MgXAg alloys. Only in case of the pure and ultra-pure Mg it can be seen that the OCP after 30 min in MEM is more anodically shifted in comparison to HBSS. The final potentials after 30 min are summarized in Table 3.

The situation at the surface after 30min OCP is shown in Fig. 5.

Even if the OCP values hardly differ, the images show visible differences after 30 min, as seen in Fig. 5. In HBSS, a difference in the amount and distribution of the HE spots and the oxide-covered area can

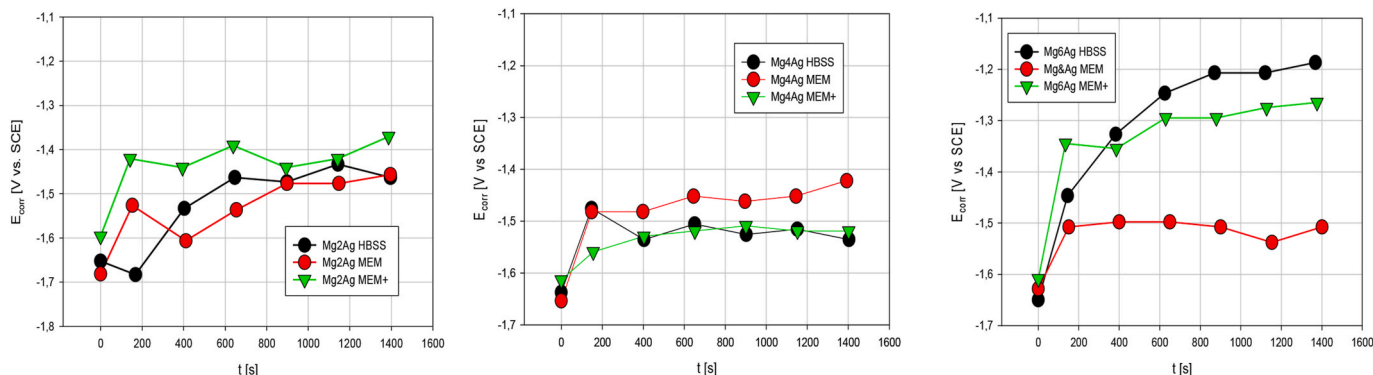


**Fig. 7.** Changes of  $E_{corr}$  of the forward scan with time for MgXAg alloys in 3 different electrolytes at 37 °C und flowing conditions.

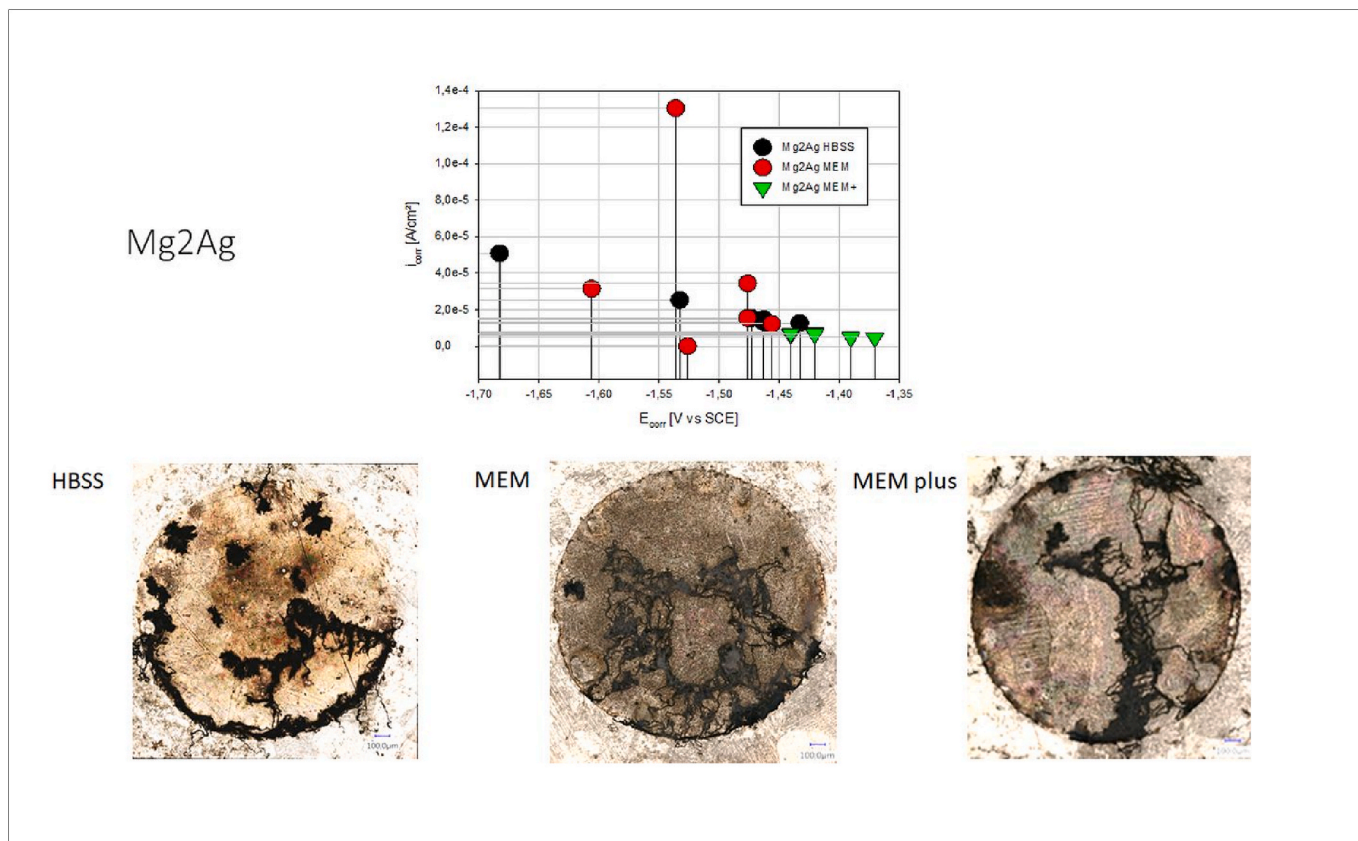


**Fig. 8a.** Comparison of  $i_{\text{corr}}$  vs.  $E_{\text{corr}}$  data from cyclic polarization (top) of Mg2Ag alloy in HBSS, MEM and MEM + together with the situation at the surface after the electrochemical measurements.

be observed. In MEM all surfaces show strong traces of oxidation, either through dark discoloration, as in the case of Mg2Ag, or paths of localized “migrating” reactions, marked with red arrows, on Mg4Ag and Mg6Ag. If NaHCO<sub>3</sub> is added to the MEM solution, the initial traces of localized oxidation are less clear and can only be seen on Mg6Ag.

### 3.2.1. Cyclic voltammetry

The cyclic voltammograms show different shapes, depending on the kind of solution as well as the kind of material, pure Mg or MgXAg alloys. There are differences related to the position of the  $E_{\text{corr}}$  and the  $i_{\text{corr}}$  data depending on the solution in which was measured. In case of the pure and ultra-pure Mg the behavior under cyclic polarization is completely different, as the curves in Fig. 6a show. In HBSS, pure Mg as well as MgXHP show no breakdown, so no additional HE (Hydrogen evolution) takes place during anodic polarization, but in MEM the typical behavior can be observed with fast hydrogen streams at some places at the surface. Characteristically, very small bubbles are created, appearing as a little stream.

In Fig. 6a to c the curves of the differently composed MgXAg alloys, polarized in different electrolytes are presented. Depending on the Ag-content some differences in the behavior can be observed. Phenomenologically, the behavior in HBSS and MEM + are comparable but slightly different to the behavior in MEM. The CV of the alloys tested in MEM (Fig. 6b) indicate that magnesium and Mg–Ag alloys exhibit hysteresis. This suggests that the material experienced pitting corrosion to some degree during immersion in the electrolytes. It is important to realize that as more silver content is included, the alloys become more prone to pitting corrosion. However, this seems to be suppressed again by adding NaHCO<sub>3</sub>, as can be seen in Fig. 6c. Mg6Ag shows pitting corrosion behavior only in the first cycle but with the passing of time, respectively the numbers of cycles, a decrease of corrosion current can be observed.

The essential data of the  $E_{\text{corr}}$  position of the forward and backward scans and the  $i_{\text{corr}}$  data respectively are presented in Table 4.

Fig. 7 shows the changes of  $E_{\text{corr}}$  depending on time, which is also related to the numbers of cycles.

In all cases an anodic shift of  $E_{\text{corr}}$  with time can be observed. Hereby the clear anodic shift of  $E_{\text{corr}}$  for Mg6Ag in NaHCO<sub>3</sub> containing electrolytes is surprising.

The data show also, that at anodically shifted  $E_{\text{corr}}$  potentials the values of  $i_{\text{corr}}$  are significantly lower as in case of more cathodically located ones, as exemplified in Fig. 8a–c.

Fig. 8a to c show the surfaces after the electrochemical polarization.

After the treatment, clear changes can be seen on the surfaces, with one exception, Mg6Ag in HBSS. There are clear traces of localized “moving” oxidation reactions, impressing as black, meandering lines. In the case of Mg4Ag in MEM plus, the areas of pitting, typical for static electrolytes, can be seen. Mg6Ag in HBSS surprises with an almost even coverage of the surface with an oxide layer without noticeable degradation spots.

### 3.3. Scanning electron-microscopy (SEM)

The SEM images (Fig. 9) of MgXAg show the surface of the specimens in three kinds of electrolytes after 200 min of electrochemical testing. MgO and Mg(OH)<sub>2</sub> are the main corrosion products around pits and cracks [25]. After electrochemical testing, all three alloys showed an irregularly spaced non-circular concavity pattern, all exhibiting a depressed surface. Mg2Ag showed both homogeneous and pitting corrosion, while Mg6Ag exhibit only mild and evenly distributed signs of pitting corrosion compared with the other two alloys in the same electrolytes. When NaHCO<sub>3</sub> is added to the MEM electrolyte with the same alloy, larger pits are clearly formed.

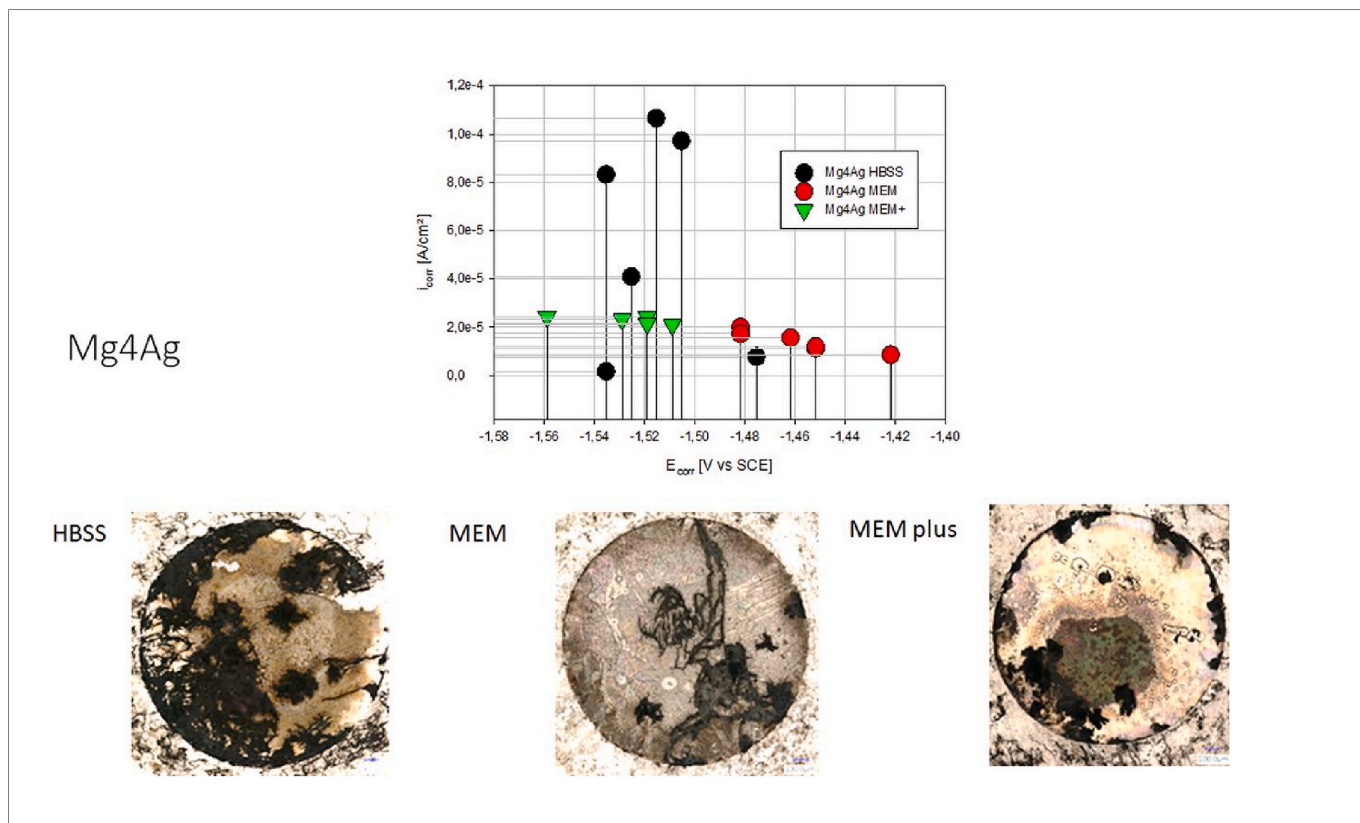


Fig. 8b. Comparison of  $i_{corr}$  vs.  $E_{corr}$  data from cyclic polarization (top) of Mg4Ag alloy in HBSS, MEM and MEM + together with the situation at the surface after the electrochemical measurements.

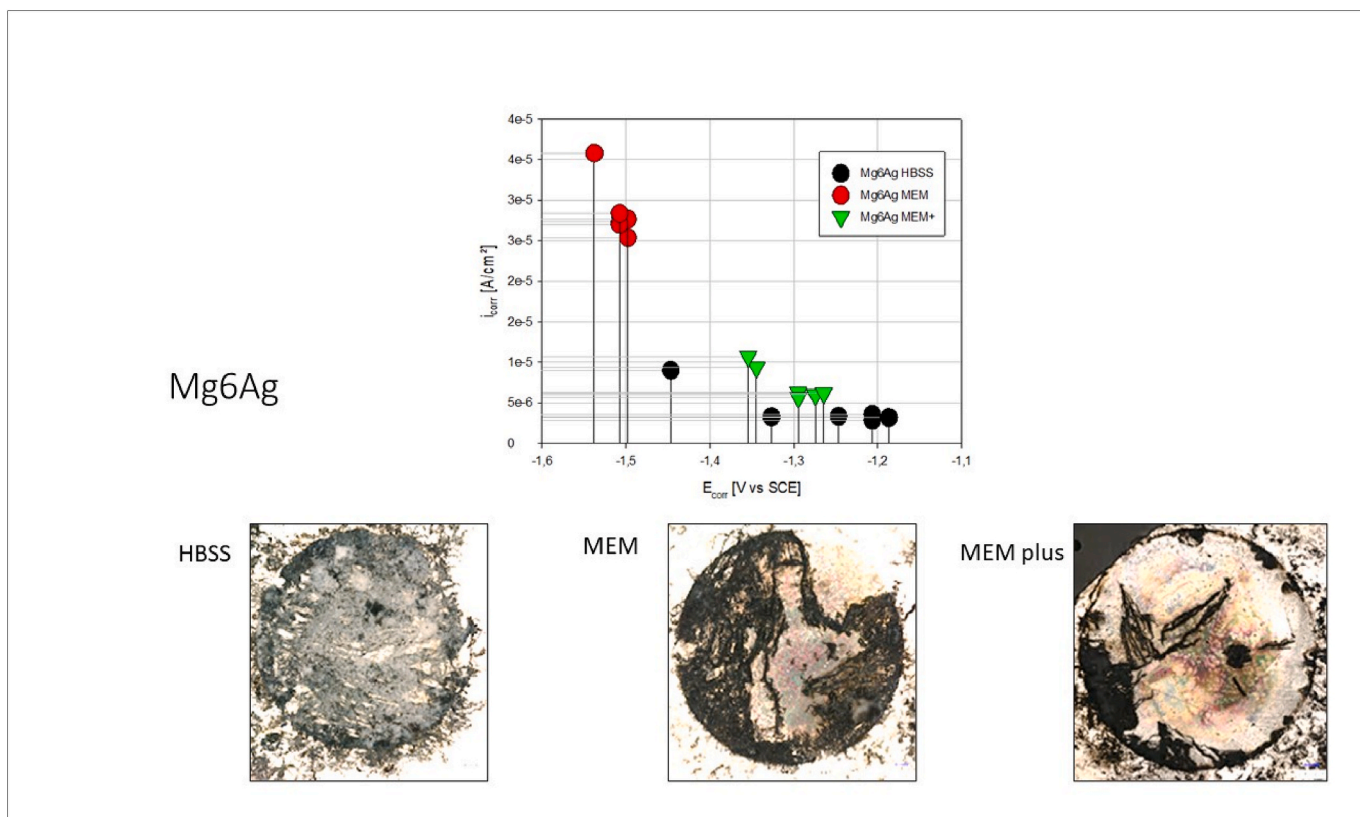


Fig. 8c. Comparison of  $i_{corr}$  vs.  $E_{corr}$  data from cyclic polarization (top) of Mg6Ag alloy in HBSS, MEM and MEM + together with the situation at the surface after the electrochemical measurements. The video microscopic view before (left) Mag: x = 150 and after (right) Mag.: x = 300; 2.5 h after the end of the experiment.

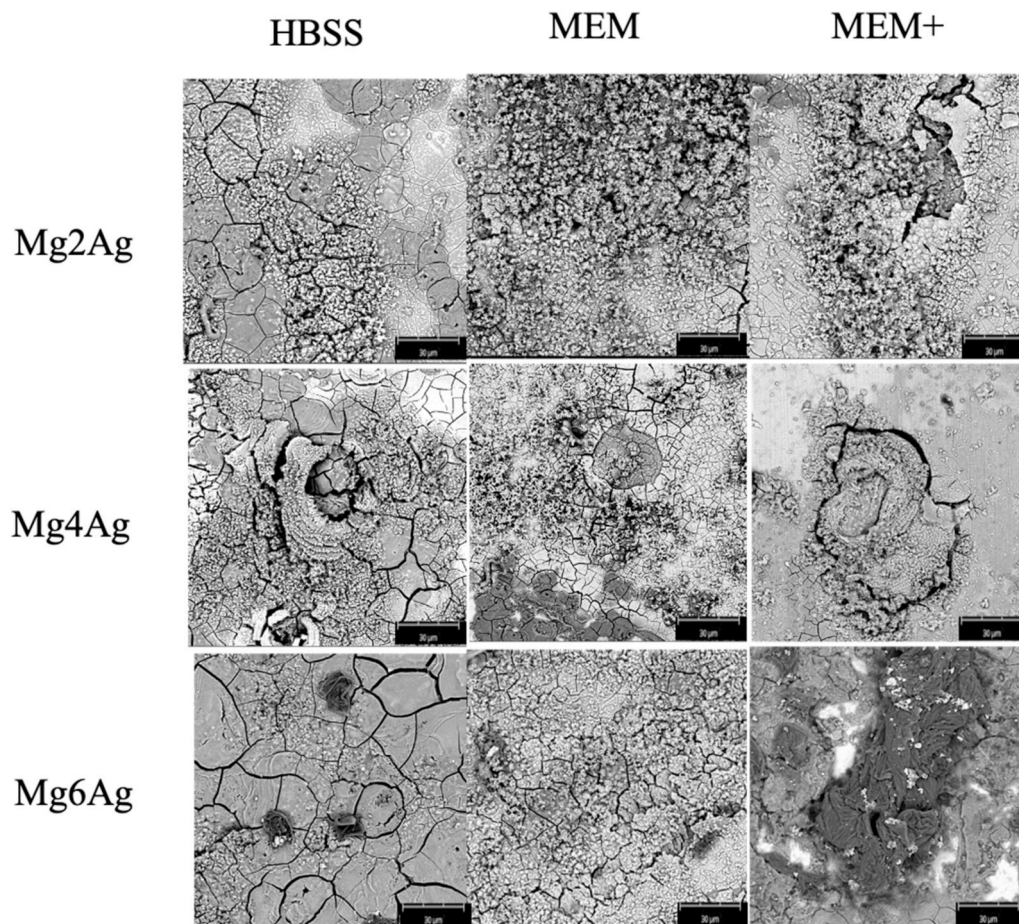


Fig. 9. Three MgXAg alloys showing special surface structure, SEM after 200mins electrochemistry experiment.

#### 4. Discussion

The exchange current densities of ( $i_{\text{corr}}$  or  $i_0$ ) represent intrinsic electron transfer rates between an analyte and an electrode [26]. These rates give insights into the composition of the analyte and the electrode and their interactions. In order to fully understand the degradation mechanism of magnesium and its alloys, the excess of HE over the Mg surface should be quantified [23].

Based on our question and aim, we expected to find a reliable correlation between the electrochemical behavior, especially when examining the exchange current density which describes the degradation rate in in-vitro environment, and the composition of the electrolytes. Secondly, we expected to investigate the influence of the visible changes including the hydrogen evolution and degradation product deposition at the surface by optical inspection during open circuit degradation and electrochemical polarization of MgXAg alloys [14,15].

As the here presented data show, a difference in the electrochemical behavior of Mg XHP and Mg pure depending on the used in-vitro solutions, HBSS and MEM, exists. To simulate the  $\text{CO}_2$  buffer activity in MEM for the measurements of the MgXAg alloys a third electrolyte, MEM+, was used.

The measurements performed in this experiment didn't clearly show any systematic factor for the difference in electrochemical behavior for MgXAg alloys. A comparison of the optical recordings before and after polarization (cyclic voltammetry) shows that a surface that is already showing active corrosion is then attacked to a greater extent. An initially only slightly oxidized surface can, however, be changed dramatically by the polarization.

This can be explained by various influences, based on the alloy

composition and its structure, such as the grain sizes and orientation as well as the chemical activity [29].

Based on our observation, no specific spots could be detected which could be fitted to the hydrogen evolution or the oxidation and precipitation of less soluble products at the surface. All analyzed surfaces have shown their own specific structure, which can be seen at the end of the treatment in Fig. 8a–c.

On the freshly polished Mg surface exposed to an aqueous solution (such as MEM or HBSS solution), corrosion proceeds on the edge of the growing patch, thereby causing the corrosion product to precipitate in the vicinity. Magnesium corrosion products have shown enhanced catalytic activity for HER [13–15].

Using the possibility to assess the forward as well as the backward scan for description of the electrochemical activity of the different MgXAg alloys, it can be shown that a slight relation between the Ag content and the anodic shift of  $E_{\text{corr}}$  at the height of  $i_{\text{corr}}$  can be seen. In case of Mg6Ag, the  $\text{CO}_2$  containing electrolytes, HBSS and MEM+, show the same activity, in contrast to  $\text{CO}_2$ -free electrolyte (MEM). But in case of Mg2Ag and Mg4Ag it is not detectable, as Fig. 10a and b show.

In every investigated case, a kind of pitting corrosion as the main form of degradation was observed at the end and it can be seen in the SEM pictures, Fig. 9. The inhomogeneity of the metal surface is one important cause of pitting corrosion [33]. The chloride ion concentration in the solution accelerates the degradation [19].

For the electrochemical assessment of the degradation of Mg and Mg-alloys these conditions are confounding [34,35]. The reduction of active reaction area as well as the link between anodic and cathodic reaction pathways make a prediction of degradation more complicated. The application of the video-optical set-up gives more information regarding

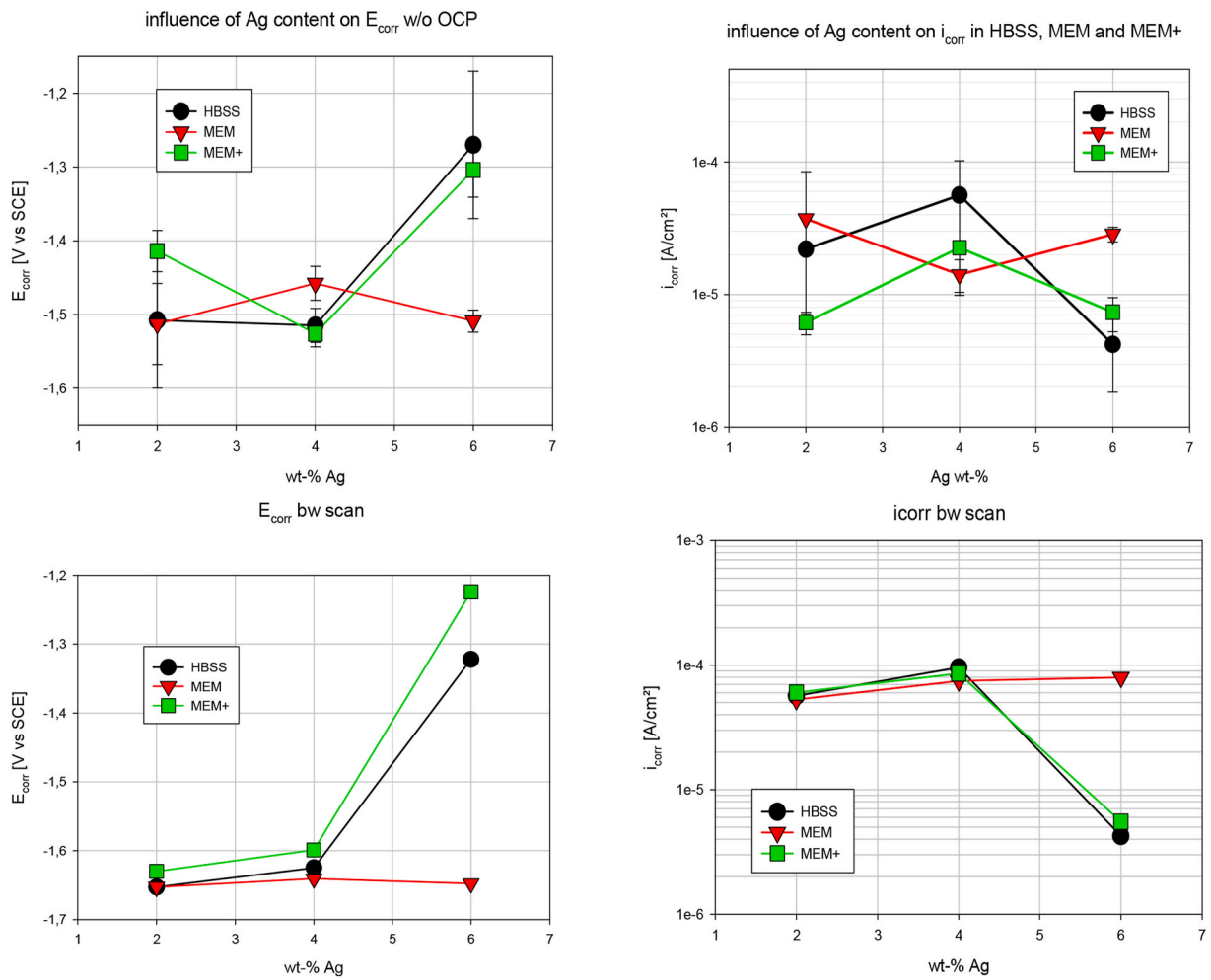


Fig. 10. Assessment of forward (top) and backward (bottom) scan for 3 different MgXAg alloys in 3 different electrolytes.

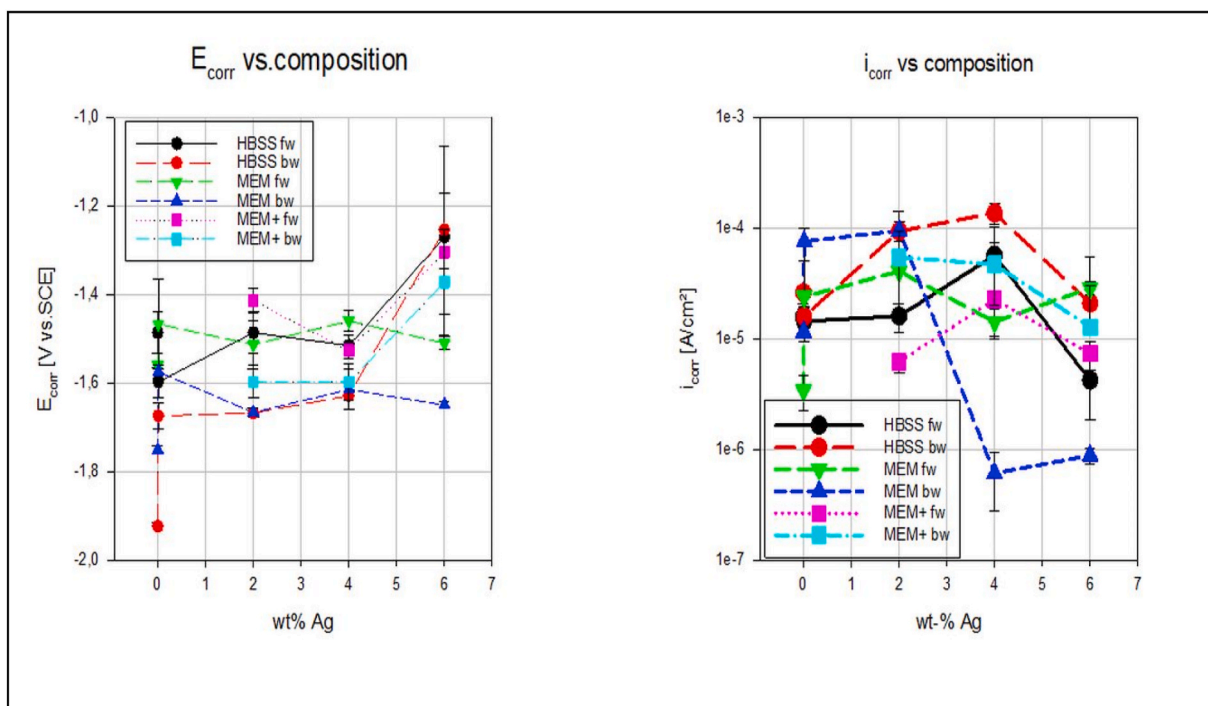


Fig. 11. Influence of the Ag-content on  $E_{corr}$  (left) and  $i_{corr}$  (right). Comparison of the data from cyclic voltammetry divided into forward and backward scan.

the influence of the composition of the electrolyte on the degradation behavior of MgXAg alloys, because the pictures during the investigation were different, namely changing positions of the oxidation, the above-mentioned meandering black lines, and also fixed positions for the hydrogen formation in the vicinity of which no visible change in the surface appearance were detected.

This makes it difficult to get a reliable picture of the degradation of Mg and Mg alloys. The visible changes on the surfaces impressed in some cases as a strong degradation and modification of the surface were not well expressed in the electrochemical data, as summarized in Fig. 11.

Due to the galvanically coupled reaction on the surface, only a trend of degradation can be given. There are more experiments necessary to find the key effect or the key location(s) of surface changes, which can be correlated to the measured electrochemical activity.

## 5. Conclusion

The varying rates of corrosion from one phase to another influenced the mechanism of pitting corrosion. The corrosion potential of Mg–Ag metallic compounds was moved in anodic direction by adding silver content. The composition of the alloy as well as the composition of the electrolyte have a significant influence on the electrochemical performance of the investigated alloys.

Most interestingly, we discovered that the silver content is a critical element in pitting corrosion protection of magnesium alloys while keeping the overall corrosion rate under control. It is also vital to pay more attention to the concept of protein evoked effects during magnesium corrosion, as it undoubtedly plays an important role in reducing both homogeneous and pitting corrosion of magnesium materials used in the body. Dependent on this performance, biodegradable implants containing MgXAg binary alloys would have a multifunctional use. In the next step the observation period can be extended, or the pH changed to monitor changes in the magnesium corrosion site. It is also our aim to track the factors influencing the trend of pitting corrosion during the reaction.

## CRedit authorship contribution statement

**Yuqiuhan Zhang:** Conceptualization, Methodology, Formal analysis, Writing – original draft, Writing – review & editing, Visualization, Validation, Formal analysis, Investigation. **Tycho Zimmermann:** Conceptualization, Methodology, Formal analysis, Writing – review & editing. **Wolf-Dieter Mueller:** Conceptualization, Formal analysis, Resources, Visualization, Writing – review & editing, Writing – original draft, Supervision, Project administration. **Frank Witte:** Resources, Project administration. **Florian Beuer:** Resources, Supervision, Project administration. **Andreas Schwitalla:** Supervision, Project administration, Review & Editing.

## Declaration of competing interest

The authors declare that they have no known competing for financial interests or personal relationships that could have appeared to influence the work reported in this paper.

## Acknowledgement

The authors would like to thank Dr. N. Hort from HZG for delivering the MgXAg specimens and Prof. Uggowitzer ETH Zurich for offering the Mg XHP and Mg pure.

## References

- [1] G.Y. Liu, J. Hu, Z.K. Ding, C. Wang, Bioactive calcium phosphate coating formed on micro-arc oxidized magnesium by chemical deposition, *Appl. Surf. Sci.* 257 (6) (2011) 2051–2057, <https://doi.org/10.1016/j.apsusc.2010.09.050>.

- [2] C. Janning, et al., Magnesium hydroxide temporarily enhancing osteoblast activity and decreasing the osteoclast number in peri-implant bone remodelling, *Acta Biomater.* 6 (5) (2010) 1861–1868, <https://doi.org/10.1016/j.actbio.2009.12.037>.
- [3] F. Witte, Acta Biomaterialia the history of biodegradable magnesium implants : a review q, *Acta Biomater.* 6 (5) (2010) 1680–1692, <https://doi.org/10.1016/j.actbio.2010.02.028>.
- [4] H.S. Brar, M.O. Platt, M. Sarntinoranont, P.I. Martin, M.V. Manuel, Magnesium as a biodegradable and bioabsorbable material for medical implants, *Jom* 61 (9) (2009) 31–34, <https://doi.org/10.1007/s11837-009-0129-0>.
- [5] B.G. Song, A. Atrens, Understanding magnesium corrosion A framework for improved alloy performance \*\*, 2003, pp. 837–858, <https://doi.org/10.1002/adem.200310405>, 12.
- [6] H. Wu, et al., Crevice corrosion – a newly observed mechanism of degradation in biomedical magnesium, *Acta Biomater.* 98 (2019) 152–159, <https://doi.org/10.1016/j.actbio.2019.06.013>.
- [7] Y. Xin, K. Huo, H. Tao, G. Tang, P.K. Chu, Influence of aggressive ions on the degradation behavior of biomedical magnesium alloy in physiological environment, *Acta Biomater.* 4 (6) (2008) 2008–2015, <https://doi.org/10.1016/j.actbio.2008.05.014>.
- [8] Z. Shi, J.X. Jia, A. Atrens, Galvanostatic anodic polarisation curves and galvanic corrosion of high purity Mg in 3 . 5 % NaCl saturated with Mg (OH) 2, *Corrosion Sci.* 60 (2012) 296–308, <https://doi.org/10.1016/j.corsci.2011.12.002>.
- [9] S. Silver, L.T. Phung, G. Silver, Silver as biocides in burn and wound dressings and bacterial resistance to silver compounds, *J. Ind. Microbiol. Biotechnol.* 33 (7) (2006) 627–634, <https://doi.org/10.1007/s10295-006-0139-7>.
- [10] B. Kwakye-Awuah, C. Williams, M.A. Kenward, I. Radecka, Antimicrobial action and efficiency of silver-loaded zeolite X, *J. Appl. Microbiol.* 104 (5) (2008) 1516–1524, <https://doi.org/10.1111/j.1365-2672.2007.03673.x>.
- [11] A.B.G. Lansdown, Silver in health care: antimicrobial effects and safety in use interactions between skin and biofunctional metals, *Curr. Probl. Dermatol.* 33 (2006) 17–34.
- [12] X. Gu, Y. Zheng, Y. Cheng, S. Zhong, T. Xi, Biomaterials in vitro corrosion and biocompatibility of binary magnesium alloys, *Biomaterials* 30 (4) (2009) 484–498, <https://doi.org/10.1016/j.biomaterials.2008.10.021>.
- [13] Y.H. Kim, et al., The effect of ball milling on the pH of Mg-based metals, oxides and Zn in aqueous media, *Met. Mater. Int.* 16 (2) (2010) 253–258, <https://doi.org/10.1007/s12540-010-0414-z>.
- [14] G. Song, Control of biodegradation of biocompatible magnesium alloys 49 (2007) 1696–1701, <https://doi.org/10.1016/j.corsci.2007.01.001>.
- [15] P. Rosemann, J. Schmidt, A. Heyn, Short and long term degradation behaviour of Mg-1Ca magnesium alloys and protective coatings based on plasma-chemical oxidation and biodegradable polymer coating in synthetic body fluid, *Mater. Corros.* 64 (8) (2013) 714–722, <https://doi.org/10.1002/maco.201206590>.
- [16] N. Ahmad, F. Feyerabend, B. Mihailova, S. Heidrich, U. Bismayer, R. Willumeit-römer, Magnesium degradation in fl uenced by buffering salts in concentrations typical of in vitro and in vivo models, *Mater. Sci. Eng. C* 58 (2016) 817–825, <https://doi.org/10.1016/j.msec.2015.09.067>.
- [17] S. Virtanen, I. Milošev, E. Gomez-Barrena, R. Trebše, J. Salo, Y.T. Kontinen, Special modes of corrosion under physiological and simulated physiological conditions, *Acta Biomater.* 4 (3) (2008) 468–476, <https://doi.org/10.1016/j.actbio.2007.12.003>.
- [18] A. Witecka, et al., In vitro degradation of ZM21 magnesium alloy in simulated body fluids, *Mater. Sci. Eng. C* 65 (2016) 59–69, <https://doi.org/10.1016/j.msec.2016.04.019>.
- [19] C. Taltavull, Z. Shi, B. Torres, J. Rams, A. Atrens, Influence of the chloride ion concentration on the corrosion of high-purity Mg , ZE41 and AZ91 in buffered Hank ' s solution. ", 2014, pp. 329–345, <https://doi.org/10.1007/s10856-013-5087-y>.
- [20] D. Hong, et al., Controlling magnesium corrosion and degradation-regulating mineralization using matrix GLA protein, *Acta Biomater.* 98 (2019) 142–151, <https://doi.org/10.1016/j.actbio.2019.05.048>.
- [21] M. Sumita, T. Hanawa, I. Ohnishi, Failure processes in biometallic materials, *Compr. Struct. Integr.* (2003) 131–167.
- [22] G. Song, *Corrosion Electrochemistry of Magnesium (Mg) and its Alloys*, Woodhead Publishing Limited, 2011.
- [23] Y. Yang, F. Scenini, M. Curioni, *Electrochimica Acta* A study on magnesium corrosion by real-time imaging and electrochemical methods : relationship between local processes and hydrogen evolution, *Electrochim. Acta* 198 (2016) 174–184, <https://doi.org/10.1016/j.electacta.2016.03.043>.
- [24] T. Zimmermann, N. Hort, Y. Zhang, W.D. Müller, A. Schwitalla, The video microscopy-linked electrochemical cell: an innovative method to improve electrochemical investigations of biodegradable metals, *Materials (Basel)*. 14 (7) (2021), <https://doi.org/10.3390/ma14071601>.
- [25] D. Tie, et al., In vitro mechanical and corrosion properties of biodegradable Mg – Ag alloys, 2014, pp. 569–576, <https://doi.org/10.1002/maco.201206903>, 6.
- [26] R. G. Kelly, J. R. Scully, D. W. Shoesmith, and R. G. Buchheit, *Electrochemical Techniques in Corrosion Science and Engineering...*
- [27] D. Tie, F. Feyerabend, W. Müller, R. Schade, K. Liefelth, K.U. Kainer, ANTIBACTERIAL BIODEGRADABLE Mg-Ag ALLOYS 25 (2013) 284–298, <https://doi.org/10.22203/eCM.v025a20>.
- [28] H. Hornberger, F. Witte, N. Hort, W. Mueller, Effect of fetal calf serum on the corrosion behaviour of magnesium alloys, *Mater. Sci. Eng. B* 176 (20) (2011) 1746–1755, <https://doi.org/10.1016/j.mseb.2011.07.018>.
- [29] J. Gonzalez, R.Q. Hou, E.P.S. Nidadavolu, R. Willumeit-Römer, F. Feyerabend, Magnesium degradation under physiological conditions – best practice, *Bioact. Mater.* 3 (2) (2018) 174–185, <https://doi.org/10.1016/j.bioactmat.2018.01.003>.

- [30] S. Fajardo, C.F. Glover, G. Williams, G.S. Frankel, Electrochimica acta the source of anodic hydrogen evolution on ultra high purity magnesium, *Electrochim. Acta* 212 (2016) 510–521, <https://doi.org/10.1016/j.electacta.2016.07.018>.
- [31] G. Williams, N. Birbilis, H.N. McMurray, Electrochemistry Communications the source of hydrogen evolved from a magnesium anode, *Electrochem. Commun.* 36 (2013) 1–5, <https://doi.org/10.1016/j.elecom.2013.08.023>.
- [32] M. Curioni, Electrochimica Acta the behaviour of magnesium during free corrosion and potentiodynamic polarization investigated by real-time hydrogen measurement and optical imaging, *Electrochim. Acta* 120 (2014) 284–292, <https://doi.org/10.1016/j.electacta.2013.12.109>.
- [33] Y. Gao, et al., Effect of stress on corrosion of high-purity magnesium in vitro and in vivo, *Acta Biomater.* 83 (2019) 477–486, <https://doi.org/10.1016/j.actbio.2018.11.019>.
- [34] N.T. Kirkland, J. Lespagnol, N. Birbilis, M.P. Staiger, A survey of bio-corrosion rates of magnesium alloys, *Corrosion Sci.* 52 (2) (2010) 287–291, <https://doi.org/10.1016/j.corsci.2009.09.033>.
- [35] F. Witte, N. Hort, F. Feyerabend, C. Vogt, “Magnesium (Mg) corrosion: a challenging concept for degradable implants,” *Corros. Magnes. Alloy.* (2011) 403–425, <https://doi.org/10.1533/9780857091413.3.403>.